

ROSETTA: ANALYSIS OF OPPORTUNITIES FOR IN-FLIGHT VERIFICATION OF THE ASTEROID FLY-BY MODE

Pablo PEREZ-ILLANA

GMV, S.A.

c/ Isaac Newton 11 PTM - Tres Cantos

E-28760 Madrid - SPAIN

pppi@gmv.es <http://www.gmv.es>

Contractor at ESA / European Space Operations Centre

Robert Bosch Str.5, D-64293 Darmstadt - GERMANY

Pablo.Perez-Illana@esa.int <http://www.esoc.esa.de>

ABSTRACT - Opportunities to check out the ROSETTA asteroid fly-by mode (AFM) are identified by pointing to other celestial targets such as at Earth swing-bys: the Moon and the Earth, and at Mars swing-by: Phobos, Deimos and Mars. This note analyses different constraints that affect the pointing process, regarding navigation camera characteristics, rotation capabilities of the probe, solar incidence on critical parts of the S/C and the high gain antenna pointing mechanism. No clear opportunity representative of the AFM is detected such that all the constraints become fulfilled simultaneously unless the tracking algorithm is commanded with certain values other than the nominal.

KEYWORDS: Attitude, tracking, in-flight verification, check-out, asteroid fly-by, swing-by, navigation camera, field of view.

1. INTRODUCTION

In order to enhance the scientific merit of the ROSETTA mission, the probe flies by the asteroid Otawara in the arc between the two consecutive Earth swing-bys and the asteroid Siwa in the arc from the second Earth swing-by to the comet Wirtanen rendez-vous (Ref. [1]). An Asteroid Fly-By Mode (AFM) has been developed in order to point the spacecraft Z axis towards the asteroid optical center throughout the fly-by, thus tracking the asteroid visible part in the field of view of the scientific instruments (Ref. [2]). The attitude guidance and control is based on a closed-loop tracking of the asteroid using navigation camera angular measurements of the asteroid optical center.

The present paper deals with the identification and analysis of opportunities to check out the asteroid tracking mode by pointing to other celestial targets, which are encountered closely enough to appear moving, such as at Earth swing-bys: the Moon and the Earth itself, and at Mars swing-by: the martian satellites (Phobos and Deimos) and Mars itself.

An obvious disadvantage of checking out the asteroid fly-by mode at the second Earth swing-by would be that the test would occur after the first operational usage of the mode at Otawara.

For every case a systematic study has been carried out analysing the different constraints that affect the pointing process, regarding navigation camera characteristics, rotation capabilities of the probe, solar incidence on critical parts of the S/C and the High Gain Antenna Pointing Mechanism (HGA - APM), as shown in section 2, where further information on spacecraft positioning and attitude is presented.

In section 3. the opportunities at first Earth swing-by are presented by means of figures related to the constraints mentioned on the previous section, firstly for the case of pointing to the Moon and secondly to the Earth. The same analysis is provided in section 4 at second Earth swing-by.

In section 5. a similar study is shown for Mars and its moons, taking now also into account the possibility of HGA coverage. For the most interesting of these cases (Deimos) a sensitivity analysis is added due to *a priori* uncertainty of predicting the times of key events.

Finally, section 6. is devoted to solutions of the problems of applying the Asteroid Fly-By Mode for cases other than the nominal. A modification in the reference direction is proposed and, for illustrative purposes, the corresponding results are shown when tracking the Moon at first Earth swing-by.

2. ROSETTA POSITION, ATTITUDE AND CONSTRAINTS AT POINTING

2.1. Spacecraft position

The orbital geometry of ROSETTA mission is already known with enough accuracy although the times of the events, such as the closest approach (= c.a.) dates, cannot be precisely predicted now. This is mainly due to the uncertainty involved in the launch window and Mars swing-by manoeuvre. For the nominal case the following data are obtained for different bodies likely to be imaged.

Table 1. Baseline Encounter Parameters¹

	Max. semiaxis (km)	Abs. magnitude V(1,0)	Closest approach date (MJD2000)	Closest approach distance (km)	Closest approach relative speed (km/s)
Earth (I)	6378	- 3.9	28/11/05 5:30:20 (2158.23)	10835.2	12.59
Moon (I)	1738	+ 0.23	28/11/05 15:25:40 (2158.64)	187800	9.36
Earth (II)	6378	- 3.9	28/11/07 15:05:55 (2888.63)	7740.2	13.73
Moon (II)	1738	+ 0.23	28/11/07 23:03:53 (2888.96)	285378	8.72
Mars	3395	- 1.51	26/08/05 19:00:52 (2064.79)	3600	8.80
Phobos	13.5	+ 11.8	26/08/05 19:14:26 (2064.80)	9070.4	9.23
Deimos	7.5	+ 12.89	26/08/05 18:29:16 (2064.77)	19011.1	8.47

Max. semiaxis (km)	Abs. magnitude V(1,0)	Closest approach date	Closest approach distance (km)	Closest approach relative speed (km/s)
--------------------	-----------------------	-----------------------	--------------------------------	--

Otawara	~2.8	+ 14.3	2006/07/11	2183	10.63
Siwa	~57	+ 8.34	2008/07/24	3500	17.04

2.2. Spacecraft attitude definition

The condition of pointing to the body optical center along the spacecraft Z axis does not fix completely the S/C attitude since a rotation around this direction is still possible. An additional restriction is therefore required to set the S/C geometrical reference frame at each time. For instance, it can be shown that imposing no rotation around Z -axis, i.e. around the direction of the relative position of the S/C w.r.t. the body target, the resulting S/C angular velocity is (see appendix):

$$\vec{\omega} = \frac{\dot{\vec{r}} \times \dot{\vec{v}}}{\dot{\vec{r}} \cdot \dot{\vec{r}}} \quad (1)$$

where:

$\dot{\vec{r}}$: S/C relative position vector w.r.t. body target

$\dot{\vec{v}}$: S/C relative velocity vector w.r.t. body target

This general formula yields the expression used e.g. in ref.3, where the relative trajectory of the S/C w.r.t. the asteroid is a straight line.

According to the Asteroid Fly-By Mode definition (Ref. [2]) the Y-axis of the S/C remains *perpendicular to the initial ground estimate of the relative velocity unit vector*. This definition determines the S/C attitude, providing that Z-axis is already defined as the tracking direction:

$$\hat{e}_z = -\frac{\dot{\vec{r}}}{|\dot{\vec{r}}|} \quad (2)$$

The Y-axis is both perpendicular to the Z-axis and to the ground estimate of the relative velocity, commanded at the beginning of the autonomous fly-by phase (Ref. [2]). (It is assumed that the chosen positive or negative direction of the Y-axis is maintained by the AFM (TBC))

$$\hat{e}_y = \mp \frac{\dot{\vec{r}} \times \dot{\vec{v}}_{comm}}{|\dot{\vec{r}} \times \dot{\vec{v}}_{comm}|} \quad (3)$$

The X-axis is such as completing the right-handed system, i.e.:

$$\hat{e}_x = \hat{e}_y \times \hat{e}_z \quad (4)$$

¹. V(1,0) is the visual magnitude when the observer is directly between the sun and the planet and the product of the sun-target distance and observer-target distance (in AU) is 1. (Data from (Ref. [10]), (Ref. [11]))

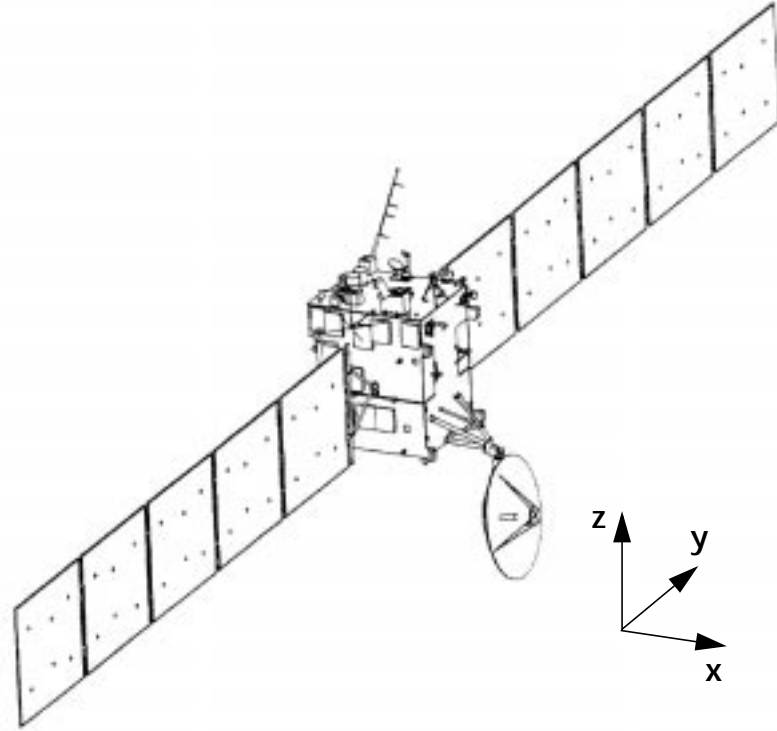


Fig. 1. ROSETTA S/C layout and geometrical reference frame

From this reference frame definition the angular rates on each axis can be computed easily according to:

$$\omega_x = -\dot{\hat{e}}_z \cdot \hat{e}_y \quad (5)$$

$$\omega_y = \dot{\hat{e}}_z \cdot \hat{e}_x \quad (6)$$

$$\omega_z = -\dot{\hat{e}}_y \cdot \hat{e}_x \quad (7)$$

Inserting eq.(2),(3) and (4) results in:

$$\omega_x = \frac{\hat{v} \cdot \hat{e}_y}{|\hat{r}|} \quad (8)$$

$$\omega_y = -\frac{\hat{v} \cdot \hat{e}_x}{|\hat{r}|} \quad (9)$$

$$\omega_z = \pm \frac{(\hat{v} \times \hat{v}_{comm}) \cdot \hat{e}_x}{|\hat{r} \times \hat{v}_{comm}|} \quad (10)$$

2.3. General Constraints

Check-out requests can be accommodated so long as they do not compromise spacecraft related activities and S/C constraints are respected.

First of all, the detected target image must remain within the ranges of allowable brightness and field of view of the navigation camera. For this purpose the evolution of the apparent angular radius of the target body will be shown, noting when the NAVCAM fov is exceeded. Moreover, the angular separation between the limbs of the planet and its corresponding moon is also monitored in order to notice any simultaneous appearance within the camera fov, which may corrupt the tracking process.

Table 2. Relevant NAVCAM characteristics

FOV	5 deg circular
CCD matrix size	1024 x 1024 pixels
Pixel dimension	13 μm
Pixel resolution	17.6 arcsec
Pixel brightness limits	+ 3 / - 5
Effective focal length	152.5 mm.

Another important aspect is the phase angle, (the angle between the spacecraft -celestial body direction and the sun - celestial body direction), not only for considerations on the target illumination but also to determine whether the sun incidence on the camera is within the forbidden range (min. 60 deg (TBC)), where straylight suppression is not guaranteed (Ref. [4]).

The solar incidence on the spacecraft is crucial since the -X face and the +, - Y faces (see fig. 1) must be protected from sun because of the presence of thermally sensitive devices, such as radiators and louvers (Ref. [6]). On the other hand, the rotation of the solar arrays, which are set along Y axis, cannot overpass its blockages at +/- 180 deg w.r.t. the reference orientation (solar array normal along the X axis according to fig. 1).

With regard to limitations on S/C steering, let us recall for instance the AAMO-715 requirement: *During asteroid fly-by, the AOCMS shall be capable of slewing the payload line of sight at a maximum rotation rate of 1 deg/sec. It shall also be compatible with a maximum acceleration of $4 \cdot 10^{-3} \text{ deg/s}^2$ at a rotation of 0.44 deg/s.* It should be taken into account that during the asteroid fly-by the slew is performed along the spacecraft minimum inertia axis (i.e. Y axis: 2700 kgm^2) by means of four reaction wheels whose capacities are 40 Nms and 0.2 Nm. Its tetrahedral configuration enables a maximum angular momentum and a maximum torque about Y axis equal respectively to 80 Nms and 0.4 Nm. For a more general case, as we are dealing with, it is checked in an analogous way the compliance of the manoeuvre rates and accelerations w.r.t. the slewing capacities around each of the three S/C axes.

Assuming omnidirectional coverage for Earth swing-bys opportunities, only the possibility of high gain antenna coverage when tracking objects at Mars swing-by is to be analysed. As shown in the next figure, the antenna pointing mechanism (APM) allows a limited Earth-pointing range, which in some regions can be reached by either of two different pairs of elevation and azimuth values.

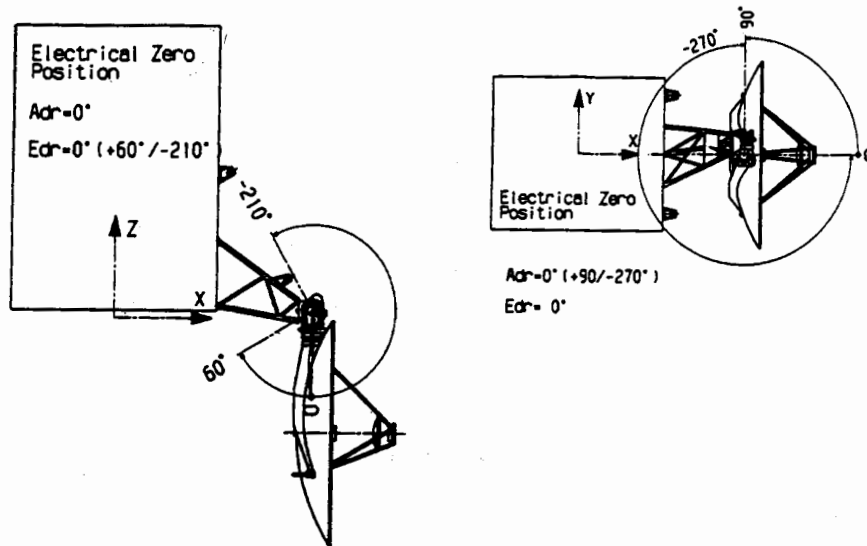


Fig. 2. HGA Elevation&Azimuth range and reference

In the following, the temporal evolution of all of these constraints will be analysed at each opportunity from 24 hours before closest approach to the planet until 24 hours later. The abscissae of the corresponding figures are expressed in hours w.r.t. the nominal time of closest approach to the respective planet. For the case of the Moon, a vertical straight line indicates the instant of closest approach to the Moon. All the angular parameters are given in degs.

3. FIRST EARTH SWING-BY

In order to analyse the opportunities throughout the first Earth swing-by it is useful keeping in mind the relative geometry of the S/C w.r.t. the celestial bodies, as shown in fig. 3 and in fig.4.

Table 3. Encounter parameters at first Earth swing-by

	Max. semiaxis (km)	Nominal closest approach date (MJD2000)	Closest approach distance (km)	Closest approach relative speed (km/s)
Earth	6378	28/11/05 5:30:20 (2158.23)	10835.2	12.59
Moon	1738	28/11/05 15:25:40 (2158.64)	187800	9.36

ROSETTA FIRST EARTH SWING-BY
FROM 1 DAY BEFORE PERICENTRE UNTIL 1 DAY AFTER
SPACECRAFT ORBIT PLANE PROJECTION

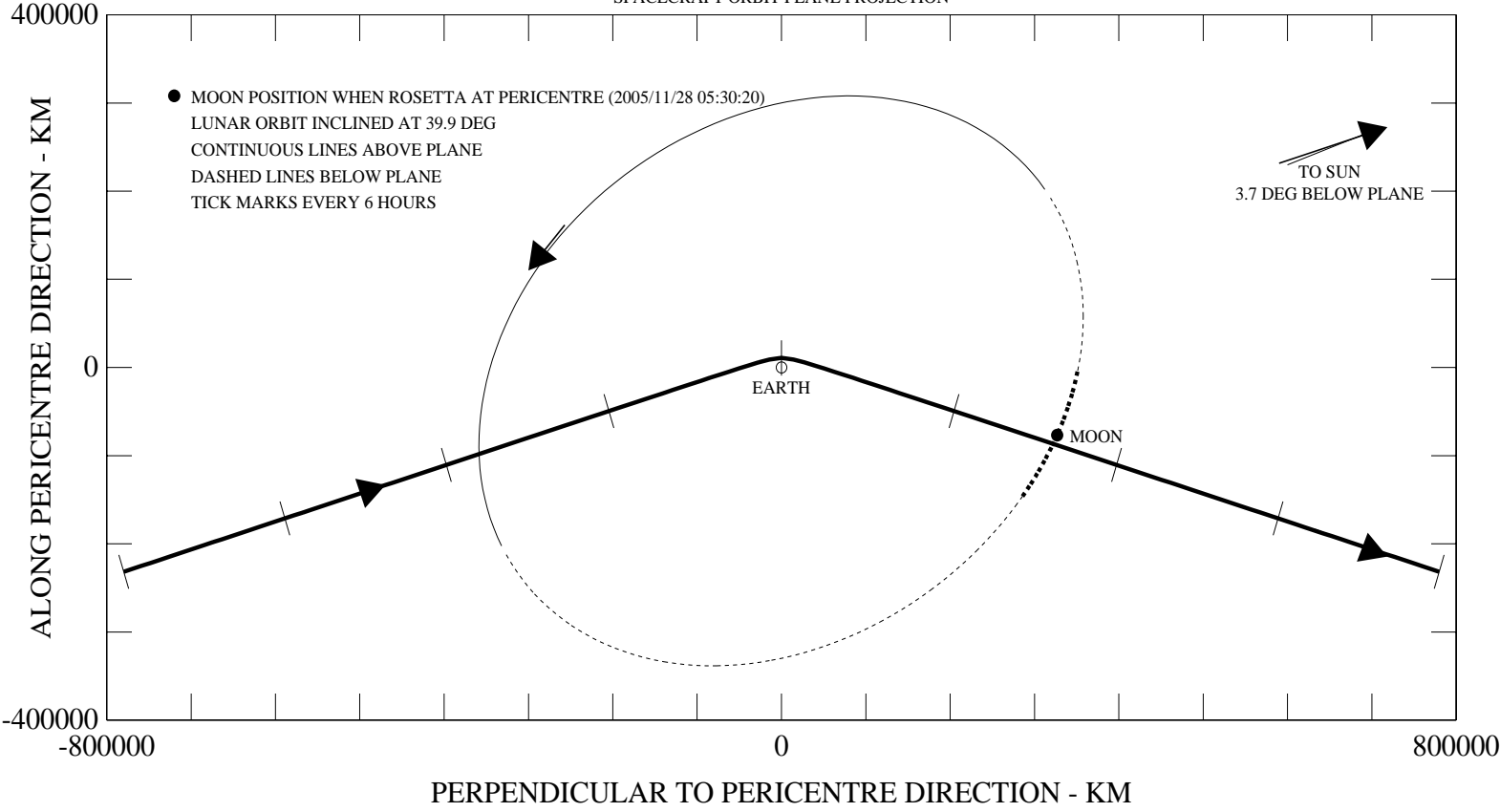


Fig. 3. First Earth swing-by projected geometry

ROSETTA TRAJECTORY RELATIVE TO THE MOON AFTER THE FIRST EARTH SWING-BY
 FROM 5 HOURS AFTER PERIGEE UNTIL 15 HOURS AFTER PERIGEE
 PROJECTION NORMAL TO ANGULAR MOMENTUM WRT MOON (AT CLOSEST APPROACH)

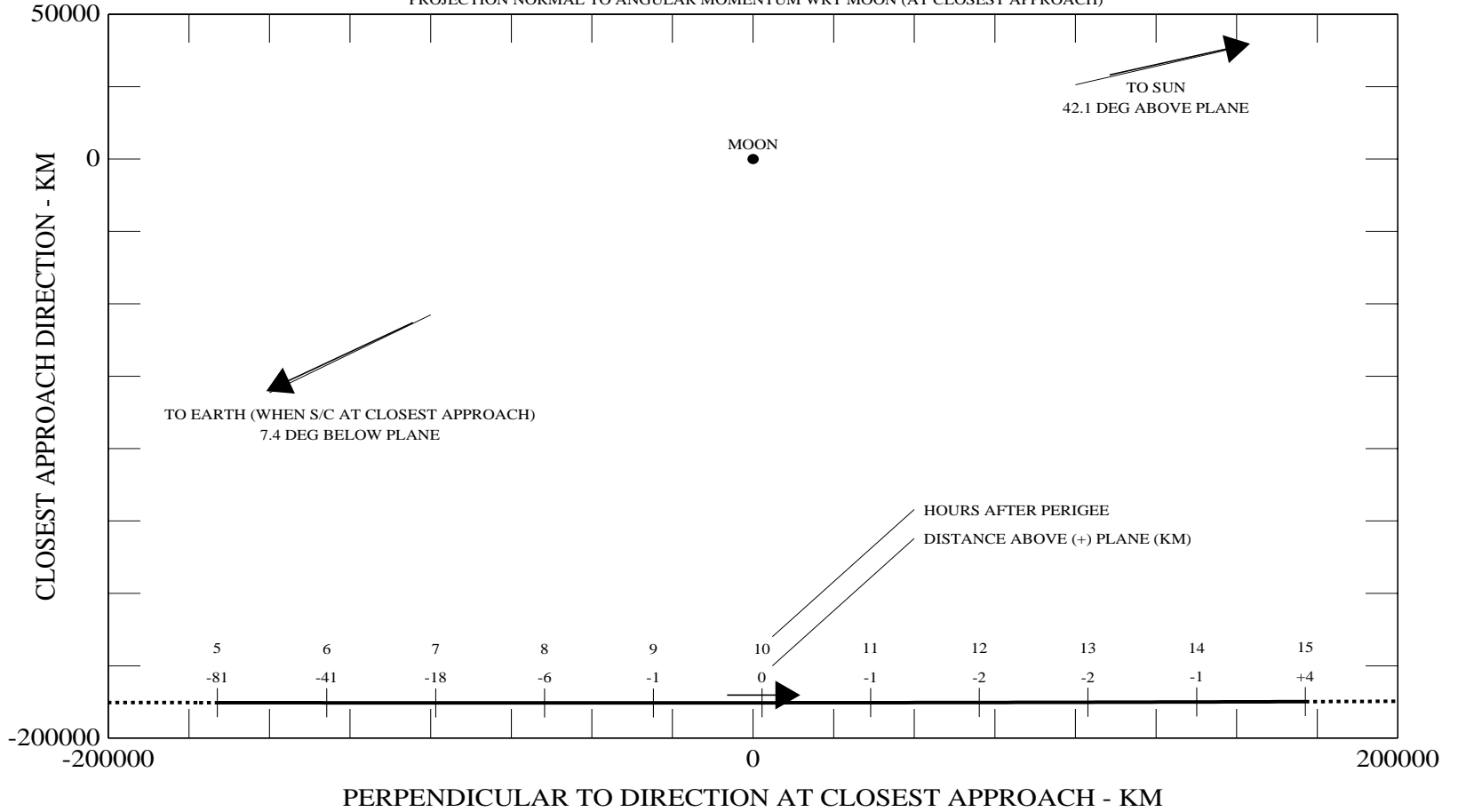


Fig. 4. Closest approach to Moon projection

3.1. Moon tracking

As shown in table 3, in the nominal case ROSETTA closest approach to the Moon takes place about ten hours after its closest approach to the Earth. At this instant the apparent angular radius of the Moon is maximum (0.53 deg) (see fig. 5). Thus, the Moon image never exceeds the NAVCAM fov. The lowest values within the studied interval are around 0.1 deg, what is translated into a projected area of about 1250 pixels.

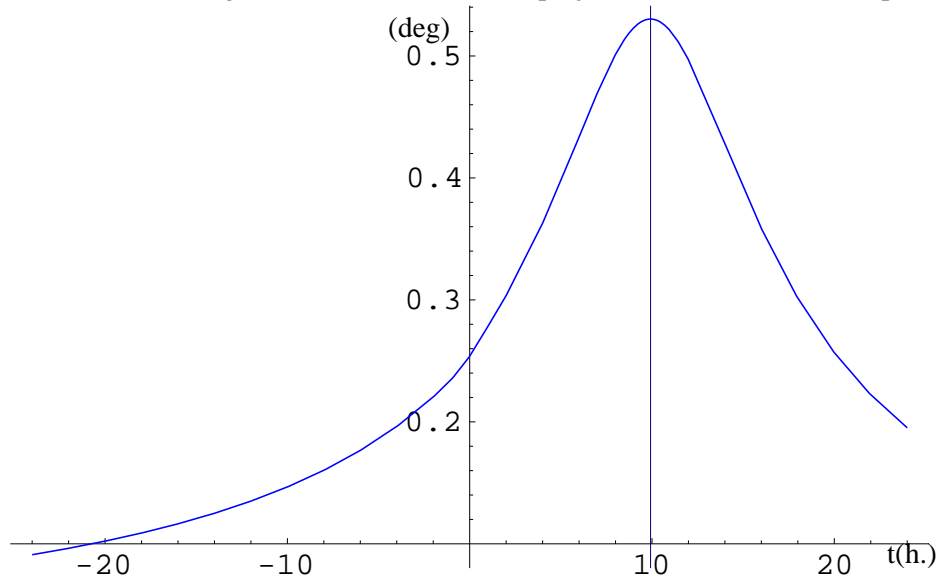


Fig. 5. Moon apparent angular radius (I)

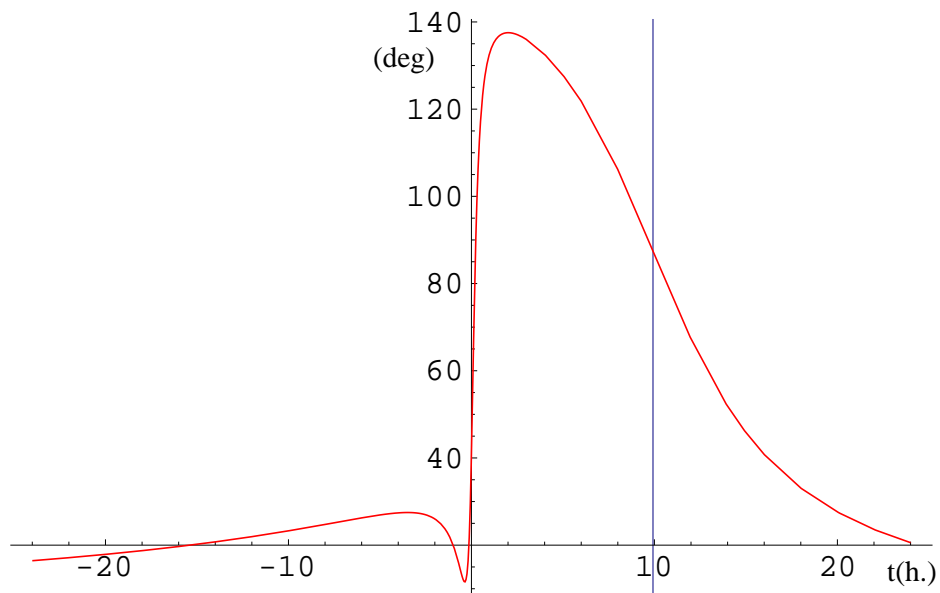


Fig. 6. Angular distance between Earth and Moon limbs (I)

From fig. 6 it may be deduced that the observed contours of the Moon and the Earth remain separated during all the tracking, and consequently there is no merging of their pictures on the fov of the NAVCAM. Fortunately, when tracking the Moon Earth image never enters the camera fov, as seen on fig. 7. Nevertheless the Earth albedo could influence the Moon tracking, especially just before closest approach to the Earth, when Earth limb is only ten degrees away from the NAVCAM fov.

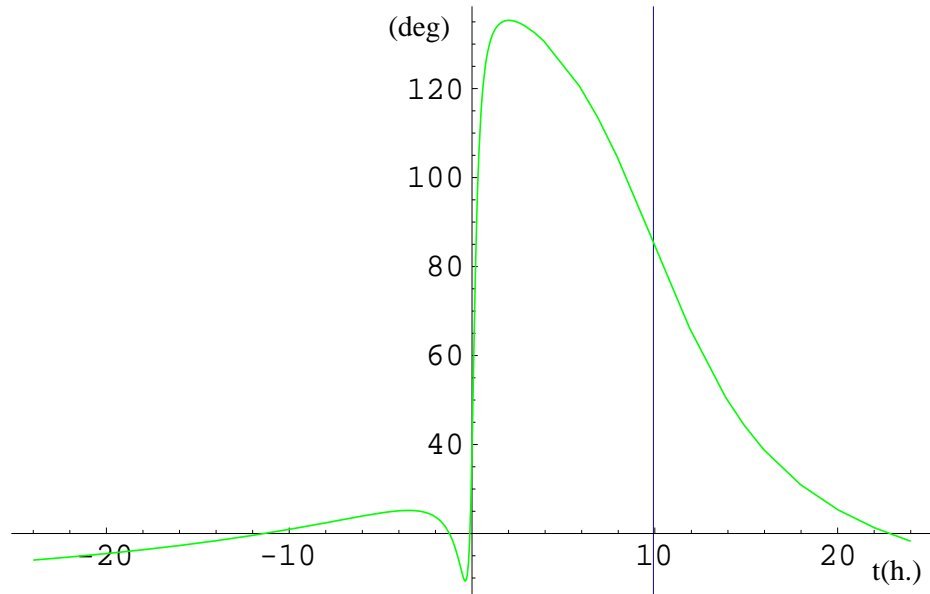


Fig. 7. Angular distance from Earth limb to Moon tracking fov (I)

The relative velocity unit vector of ROSETTA w.r.t. the Moon at its closest approach to the Moon has been taken as the commanded direction of reference for the definition of the on-board reference frame (see eq.2). Spacecraft rotation due to pointing to Moon according to AFM yields angular rates on the three S/C axis without exceeding the reaction wheels capabilities in any case. The maximum peak is lower than 0.003 deg/s and is reached on the Y-axis at the closest approach to the Moon (fig. 8.), while the other rates (on X and Z axis) are only present around the closest approach to the Earth. These rates vanish on coming closer to the Moon since here the relative trajectory ROSETTA-Moon is well approximated by a straight line (fig. 4) and, therefore, the relative velocity unit vector is almost equal to that commanded at the beginning.

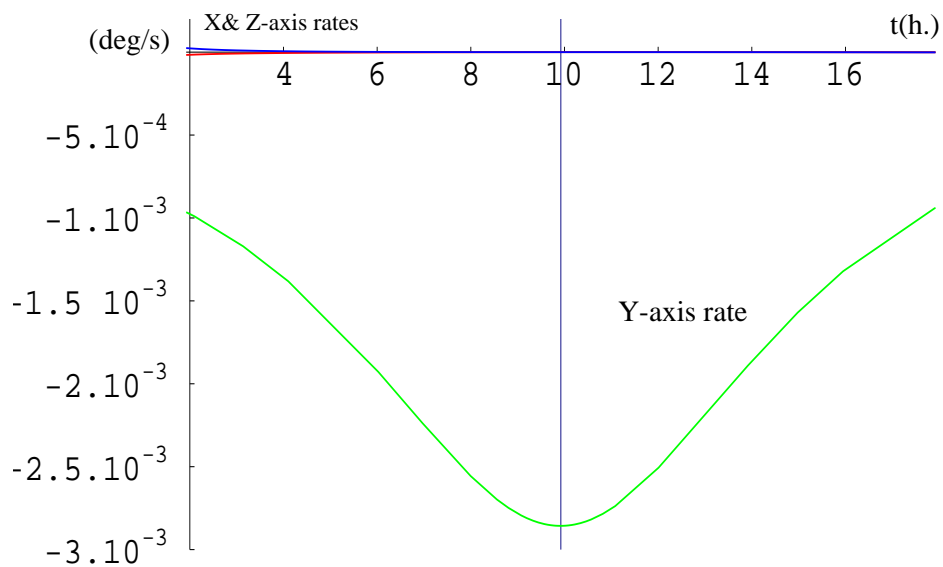


Fig. 8. Angular rates when pointing to Moon (I)

The subsequent angular acceleration is displayed in fig. 9. in terms of the derivatives of the previous angular rates and they are also below the limit of $4 \cdot 10^{-3} \text{ deg/s}^2$.

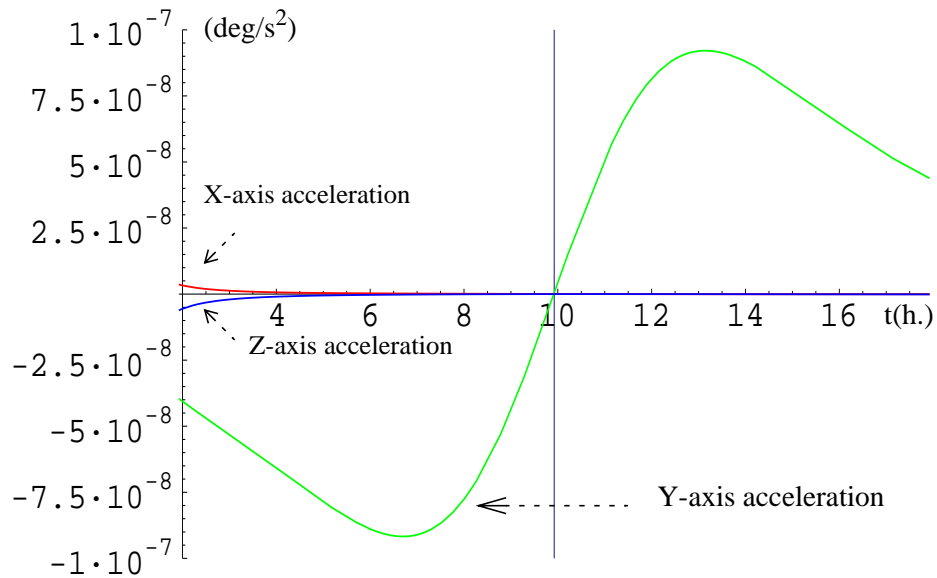


Fig. 9. Angular accelerations when pointing to Moon (I)

The geometrical projection of the first ROSETTA Earth swing by (fig. 3) explains the evolution of the phase angle (fig. 10): up to a few hours before the closest approach to the Moon the solar incidence on the navigation camera is undesirable since sun appears near the line of sight of the NAVCAM.

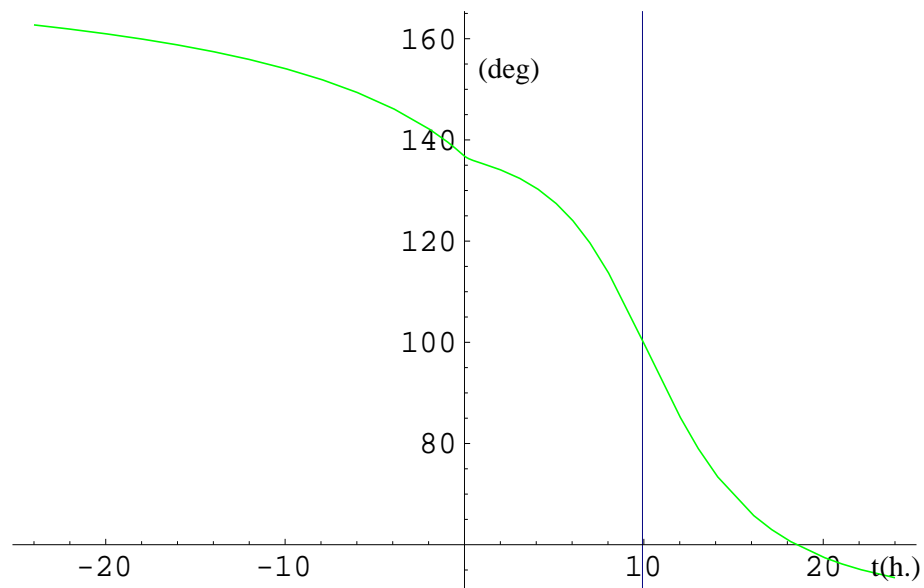


Fig. 10. Phase angle w.r.t. Moon (I)

After closest approach to the Earth, the configuration is more advantageous and the illumination of the Moon also improves. An estimate of the brightest pixel magnitude has been performed following refs. 7, 8, 9, which apply Lambert scattering of sunlight and assume that a pixel projects onto a small plane surface element

$$m_{pix} = m_{sun} + 2.5 \log \left[\frac{\pi \left(\frac{r_h f}{1AU w_{pix}} \right)^2}{p_B \cos \gamma} \right] \quad (11)$$

where:

m_{Sun} is the magnitude of the Sun at 1 AU distance,

r_h is the heliocentric distance to the Moon,

f is the effective focal length of the camera,

p_B is the Bond Albedo of the Moon ($p_B = 0.067$ (Ref. [10])),

w_{pix} is the length of a pixel side and

γ is the angle between the Sun direction and the normal to the surface of the illuminated object.

The brightest part of the Moon is at the middle of the illuminated edge. When this part cannot be projected back on the field of view of the camera then the brightest pixel corresponds to $\gamma = \alpha - 90 \text{ deg} + \text{Moon apparent angular radius}$, where α is the solar phase angle, (for instance, initially the brightest pixel magnitude is about -1.2), but once that $\gamma = 0$ is achieved (around the closest approach to the Moon) the absolute maximum magnitude is kept equal to -2.5. We recall that these values are far from the NAVCAM illumination limits -5/+3, therefore neither too bright nor too faint.

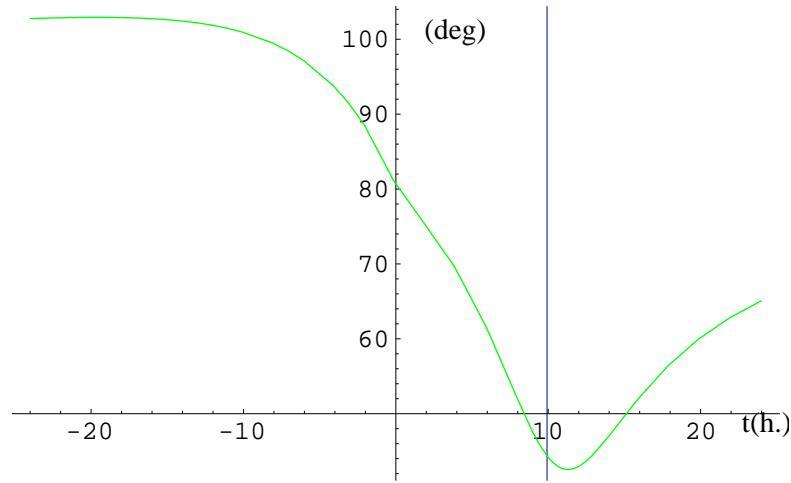


Fig. 11. Angle between sunwards direction and X- axis when pointing to Moon (I)

As presented in section 2, Y-axis direction was set according to the tracking requirements defined on the AFM. Its orientation is chosen¹ here so that the -X face becomes protected from sun during the interval with the most

$$\hat{e}_y = - \frac{\hat{r} \times \hat{v}_{comm}}{|\hat{r} \times \hat{v}_{comm}|} \quad (12)$$

favourable conditions of solar incidence on the NAVCAM, i.e. from a few hours before closest approach to the Moon onwards. (See fig. 11). During this period the solar array (SA) rotation is also far from its blockages at +/- 180 degs, as shown in fig 12.

¹. Providing that allowed by AFM. (TBC)

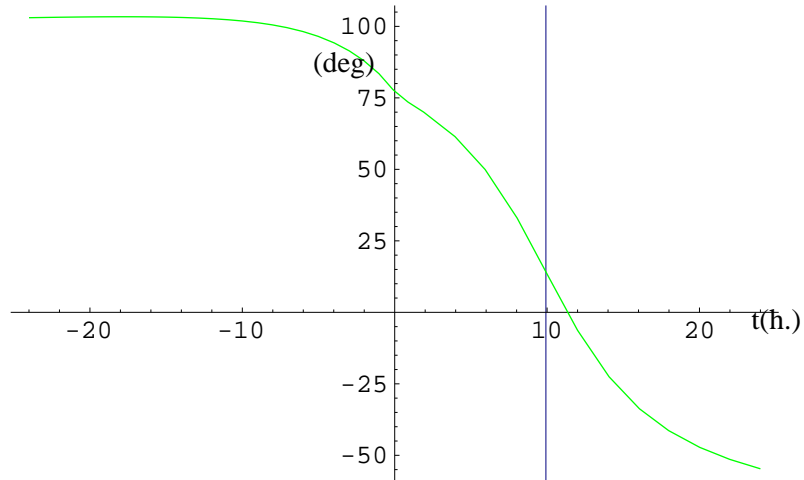


Fig. 12. Angle between SA normal and X- axis when pointing to Moon (I)

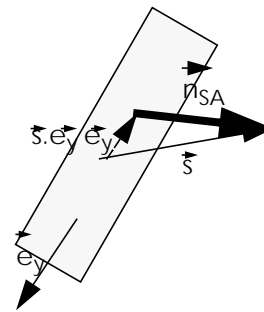
Solar array rotation around Y-axis is given by the condition of maximum power, i.e the angle between SA normal and sun direction is minimized. Mathematically, the SA normal \vec{n}_{SA} is defined by:

$$\vec{n}_{SA} = \frac{\vec{s} - (\vec{s} \cdot \vec{e}_y)\vec{e}_y}{|\vec{s} - (\vec{s} \cdot \vec{e}_y)\vec{e}_y|} \quad (13)$$

where:

\vec{s} : sunwards direction unit vector

\vec{e}_y : Y-axis unit vector



The resulting off-pointing is acceptable at a heliocentric distance of 1AU in order to provide sufficient power. Note that ROSETTA's solar arrays are designed to supply enough power for full science operations at a S/C-sun distance of about 3.5 AU.

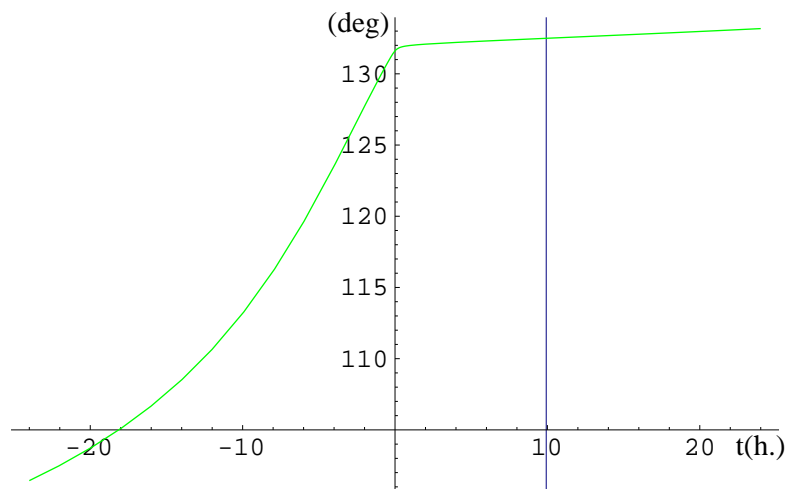


Fig. 13. Angle between sunwards direction and Y- axis when pointing to Moon (I)

As followed from the definition of the normal direction to the solar array, the angle δ between sunwards direction and the Y-axis is obtained from:

$$\cos \delta = \hat{s} \cdot \hat{e}_y \quad (14)$$

Unfortunately fig.13 shows that in the zone of interest, around closest approach to the Moon, the solar incidence angle on -Y face is about 45 deg, which is not suitable thermally.

3.2. Earth tracking

In principle during the first Earth swing-by an alternative check-out strategy could be to point to Earth instead of to Moon. Observing the evolution of the Earth angular radius (fig. 14) it is noted that the fov of the NAV-CAM becomes exceeded for eight hours around the closest approach time, so the period of study is divided into two separate intervals.

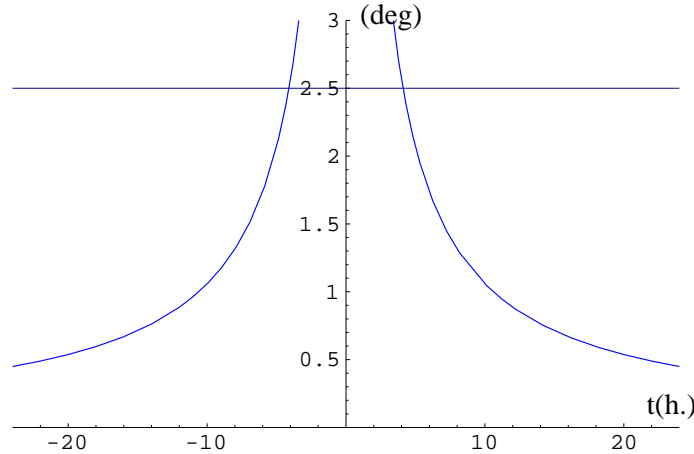


Fig. 14. Earth apparent angular radius (I)

Tracking the Earth during the interval prior to four hours before c.a. is unsuitable because of phase angle next to 180 deg (fig. 15). On the other hand pointing to Earth in the second interval avoids this drawback but it is not clear how the AFM algorithm behaves when tracking is initiated after closest approach. Furthermore, an estimation of the intensity of the brightest pixel leads to magnitudes about -4.5, which is much closer to the camera limit than in the case of the Moon.

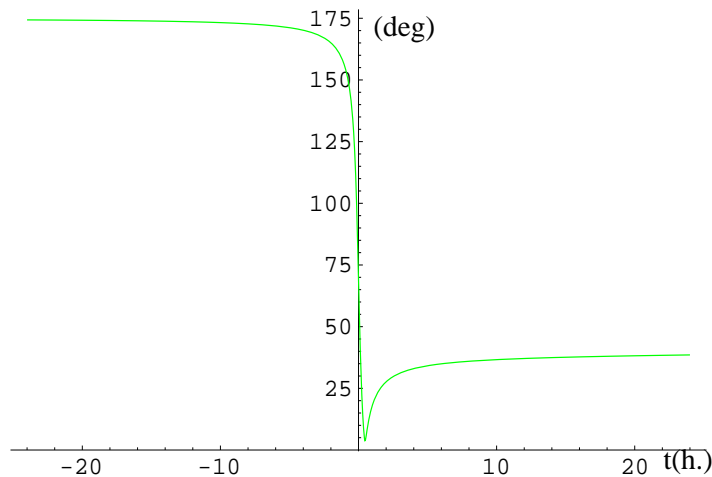


Fig. 15. Phase angle w.r.t. Earth (I)

During that second interval, i.e from four hours after closest approach onwards, the angular rates are kept below the limits, as shown in fig.16.

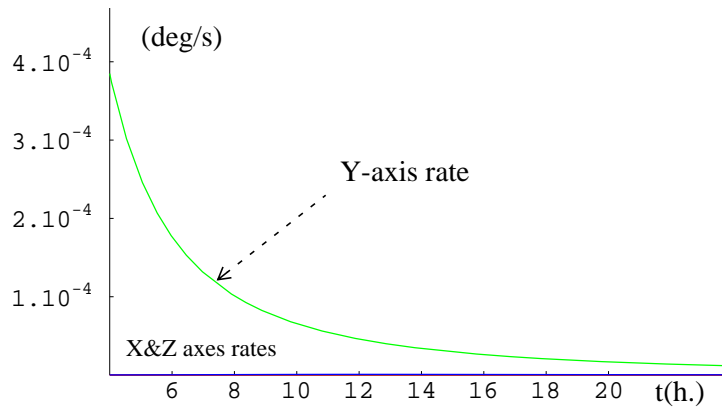


Fig. 16. Angular rates when pointing to Earth (I)

During this interval the phase angle is favourable, sun incidence on -X side is far from the restrictions when selecting the correct orientation of Y axis (fig. 17) and, finally, solar incidence on +/- Y faces and solar array orientation is adequate since the offsetting turns out to be only around 4 deg. However, as already mentioned, tracking a receding target may not be well-suited to check-out the Asteroid Fly-by Mode.

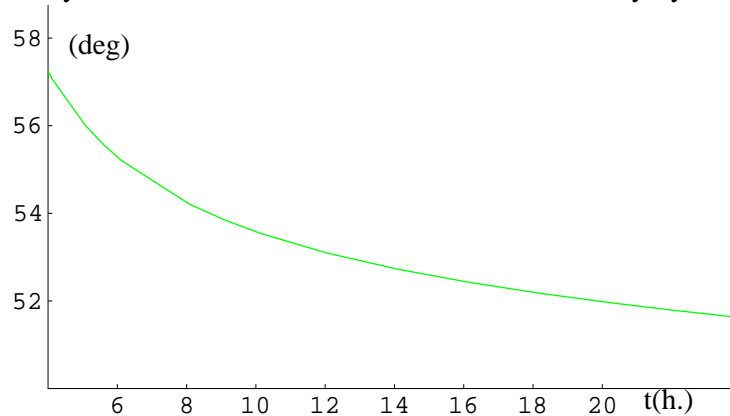


Fig. 17. Angle between sunwards direction and X- axis when pointing to Earth (I)

4. SECOND EARTH SWING-BY

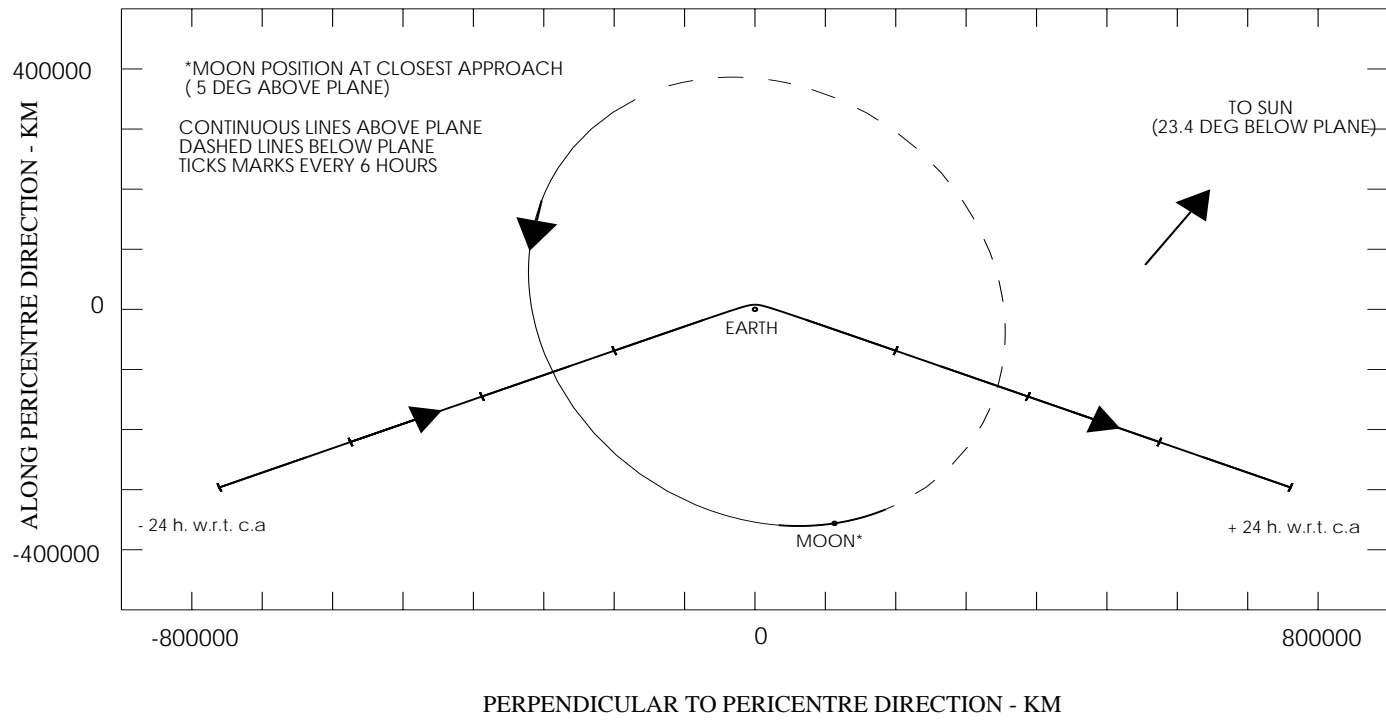
First of all, the corresponding projected geometry is shown in fig. 18

Table 4. Encounter parameters at second Earth Swing-by

	Max. semiaxis (km)	Abs. magnitude V(1,0)	Closest approach date (MJD2000)	Closest approach distance (km)	Closest approach relative speed (km/s)
Earth	6378	- 3.9	28/11/07 15:05:55 (2888.63)	7740.2	13.73
Moon	1738	+ 0.23	28/11/07 23:03:53 (2888.96)	285378	8.72

ROSETTA SECOND EARTH SWING-BY
FROM 1 DAY BEFORE CLOSEST APPROACH UNTIL 1 DAY AFTER.
SPACECRAFT ORBIT PLANE AT CLOSEST APPROACH PROJECTION

Fig. 18. Second Earth swing-by projected geometry



4.1. Moon tracking

In this case closest approach to the Moon takes place eight hours after closest approach to the Earth. The brightness and projected area of the Moon image are within the NAVCAM ranges.

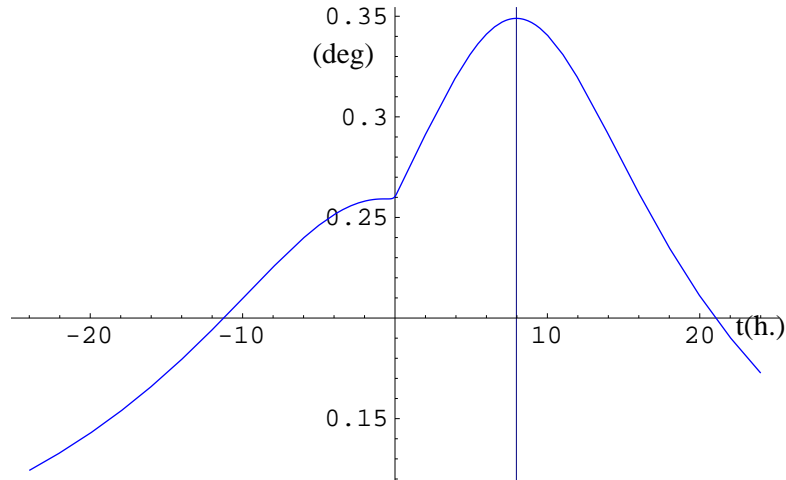


Fig. 19. Moon apparent angular radius (II)

The horizontal slope of the apparent angular radius around closest approach to the Earth is explained by the geometrical configuration during this second Earth swing-by shown in fig. 18. The Moon passes behind the Earth at almost the same time that ROSETTA reaches the closest approach to the Earth. Consequently, it is not feasible to track the Moon at this moment, as shown in fig20.

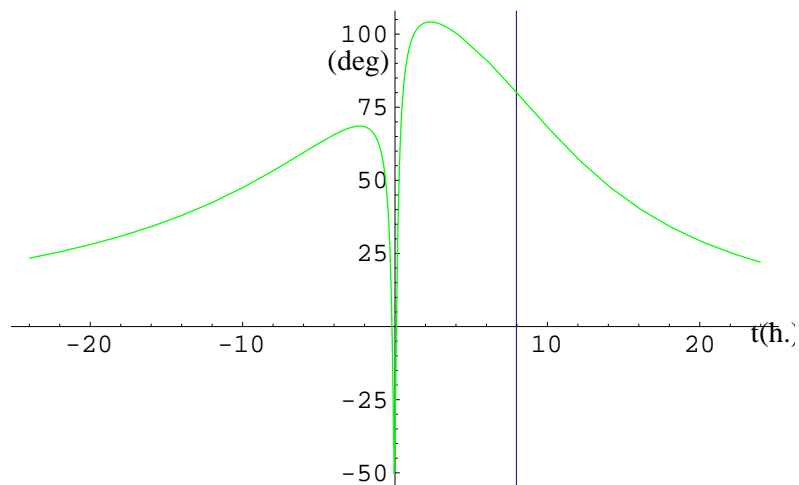


Fig. 20. Angular distance from Earth limb to Moon tracking FOV (II)

As followed from fig. 21, the lowest values of the phase angle are reached near the closest approach to the Moon.

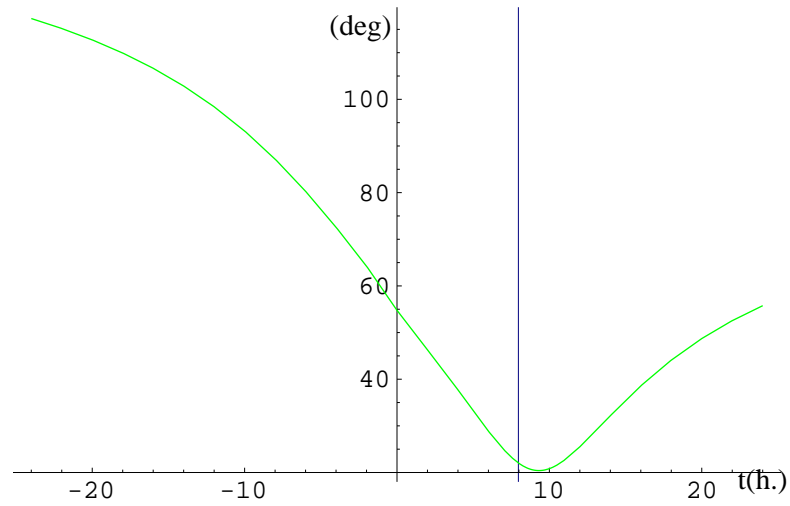


Fig. 21. Phase angle w.r.t. Moon (II)

It has been also checked that the corresponding rates and accelerations are compatible with the reaction wheels capabilities, assuming again that the commanded direction is the relative velocity unit vector of closest approach to the Moon.

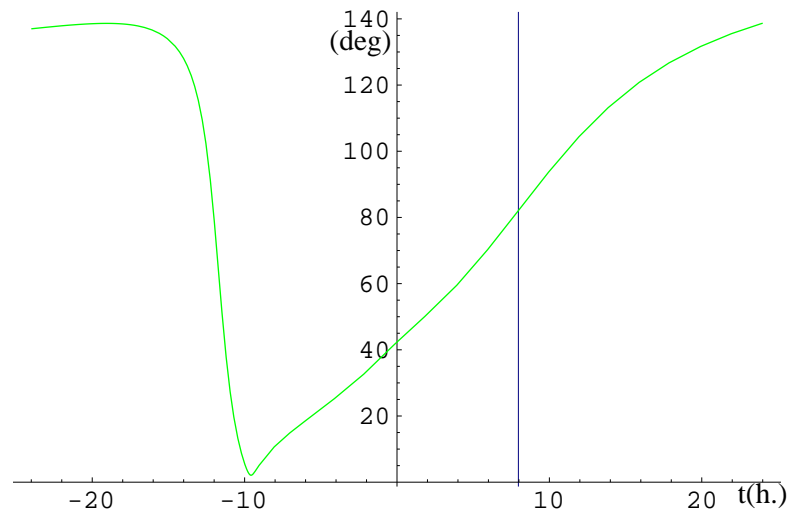


Fig. 22. Angle between sunwards direction and X- axis when pointing to Moon (II)

-X Face is only wholly protected approximately from -12 h to +10 h w.r.t. closest approach to the Earth (fig. 22) while solar incidence on +/- Y-face is only optimum (90 deg) at -10 h, changing rapidly around this time, (see fig. 23), which indicates that tracking period would be more or less restricted depending on the maximum tolerable solar elevation above the +/- Y-faces. The solar elevation above +/- Y faces around closest approach to the moon is about 20 deg.

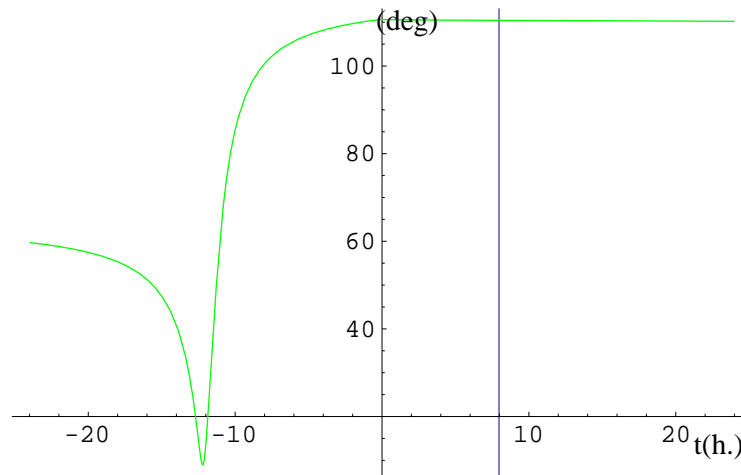


Fig. 23. Angle between sunwards direction and Y- axis when pointing to Moon (II)

4.2. Earth tracking

As for the first Earth swing-by, constraints fulfilment would force to point to Earth when it is receding: effective AFM tracking feasibility on this conditions is to be determined.

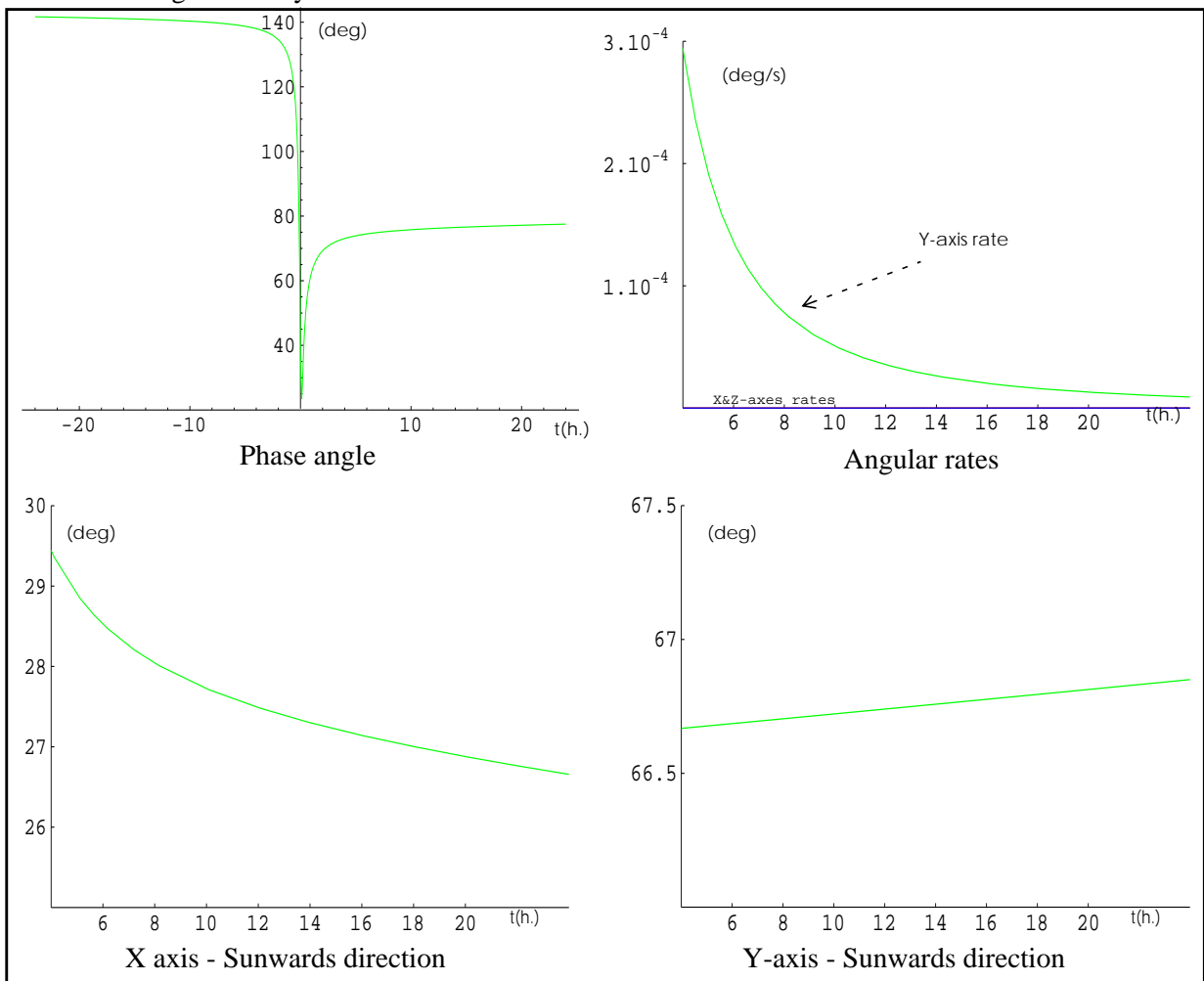


Fig. 24. Angular rates and sun incidence when tracking the Earth (II)

5. MARS SWING-BY

The geometrical configuration of the S/C w.r. t. Mars and its moons for the nominal case is shown in fig.25 (extracted from ref.4)

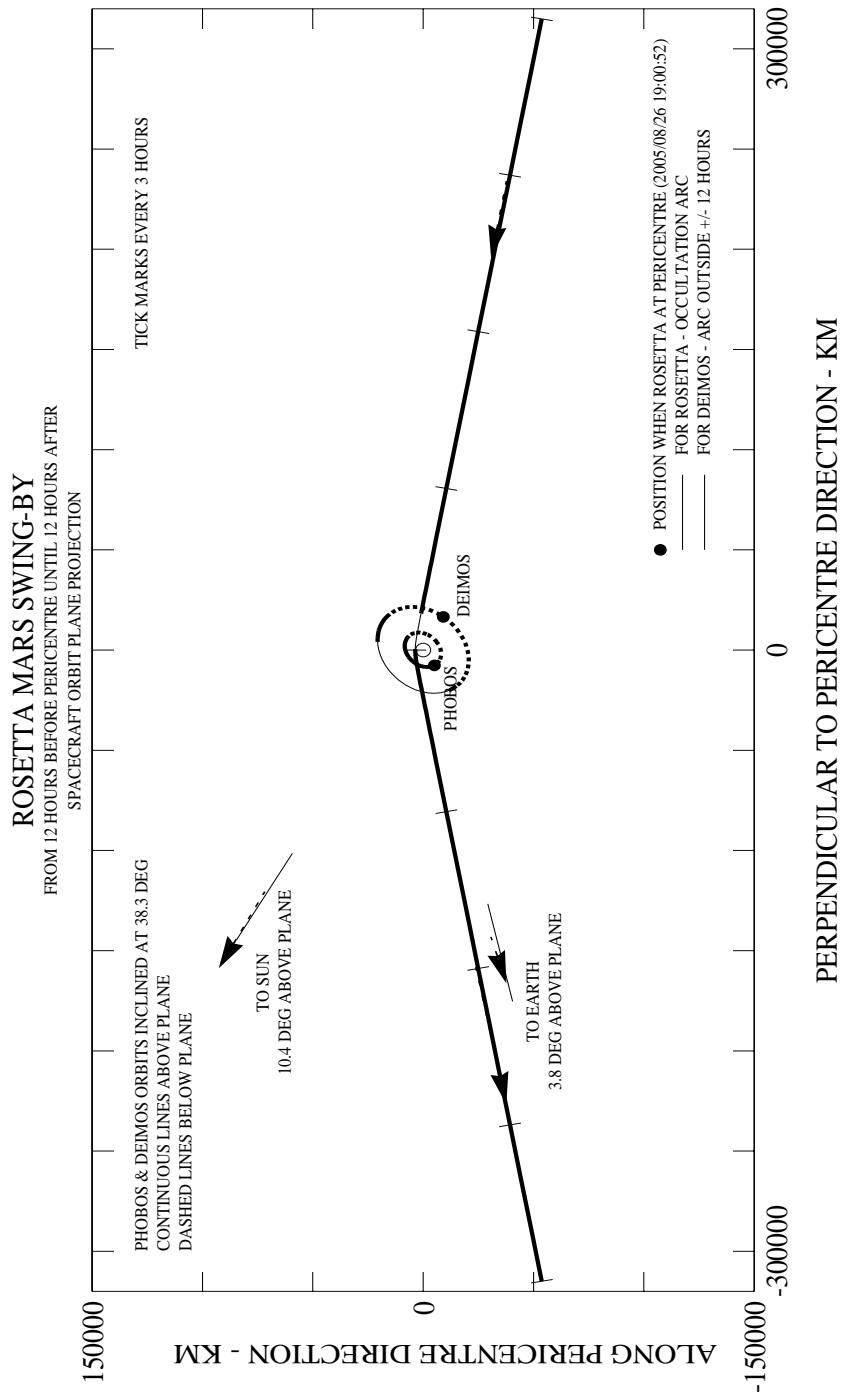


Fig. 25. Mars swing-by projected geometry

Table 5. Encounter parameters at Mars swing-by.

	Max. semiaxis (km)	Nominal closes approach date (MJD2000)	Closest approach distance (km)	Closest approach relative speed (km/s)
Mars	3395	26/08/05 19:00:52 (2064.79)	3600	8.80
Phobos	13.5	26/08/05 19:14:26 (2064.80)	9070.4	9.23
Deimos	7.5	26/08/05 18:29:16 (2064.77)	19011.1	8.47

5.1. Mars tracking

During Mars swing-by, the entire image of the planet cannot fit within the camera fov for some hours around the closest approach (see fig. 26 from -3 h to +3 h)

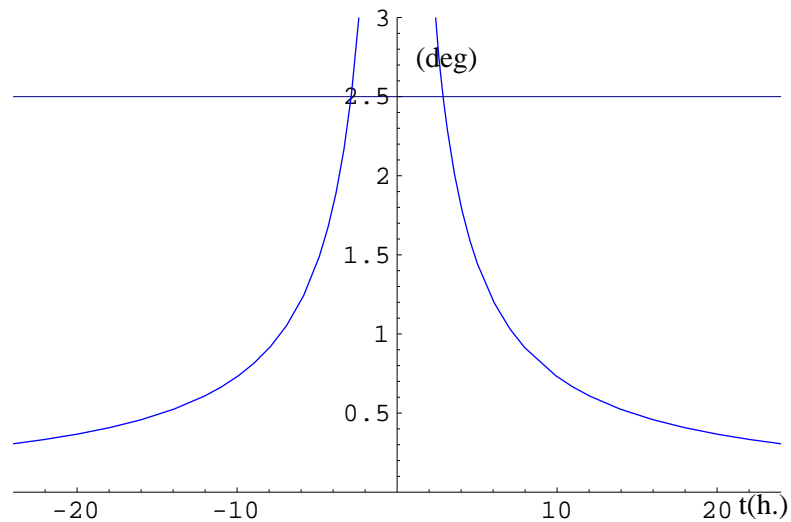


Fig. 26. Mars apparent angular radius

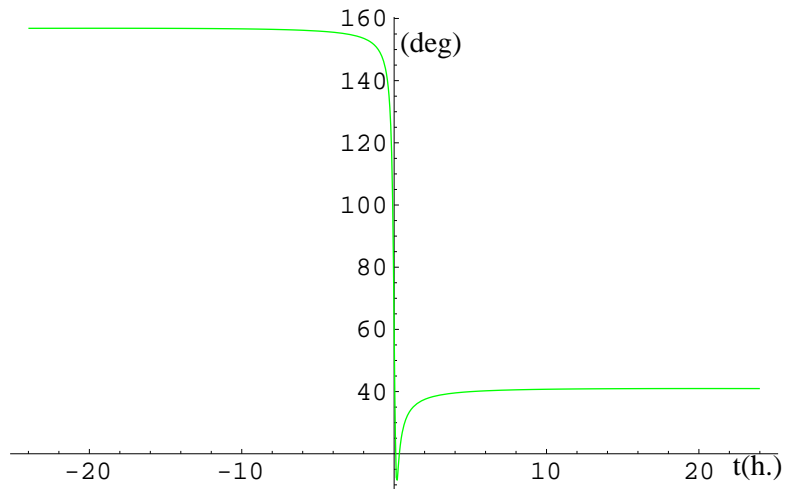


Fig. 27. Phase angle w.r.t. Mars

The phase angle is only appropriate after the closest approach (fig. 27), and by correct choice of the Y-axis orientation, the -X face is kept in shadow during the selected interval (i.e. from $t = +3$ h onwards) (see fig. 28).

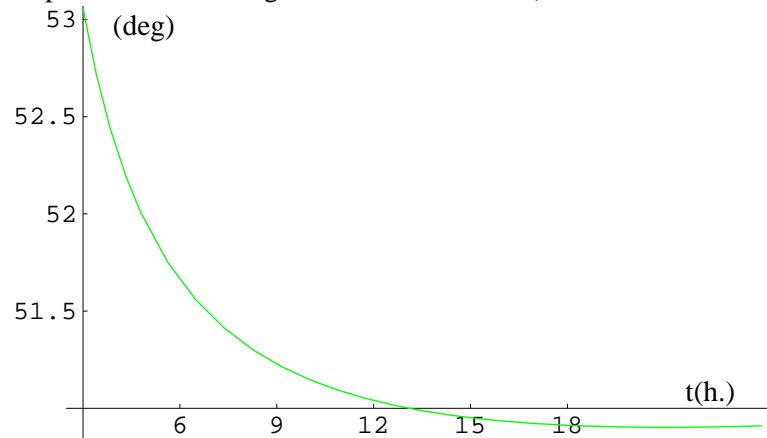


Fig. 28. Angle between sunwards direction and X-axis when pointing to Mars

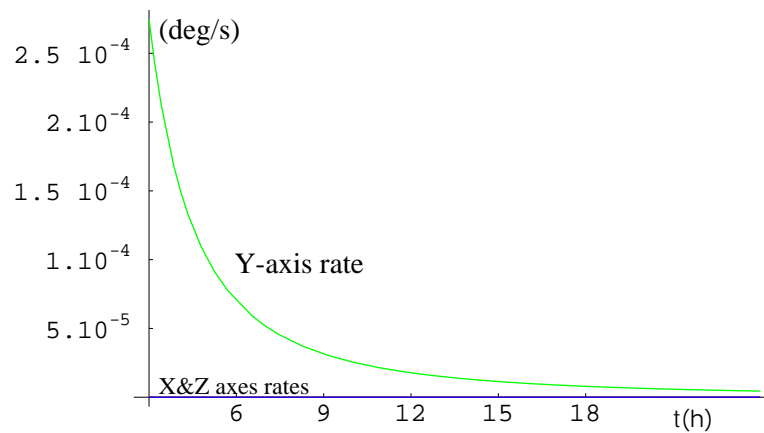


Fig. 29. Angular rates when pointing to Mars

Angular rates and accelerations remain within allowed ranges during the selected interval from $t = +3$ h onwards, as shown in fig.29. (The relative velocity unit vector at closest approach to Mars has been taken as the

commanded reference direction). The angle between Y-axis and sunwards direction remains at about 80 deg (see fig.30), i.e. sun incidence on +Y face is ten degrees.

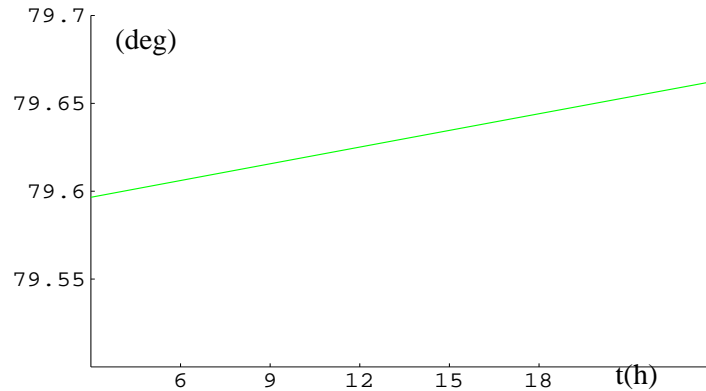


Fig. 30. Angle between sunwards direction and Y-axis when pointing to Mars

In comparison to the case of the Earth a new aspect is the communication link via the High Gain Antenna. According to fig. 2, for each Earth-pointing orientation two different combinations of the pointing angles (denoted by "azimuth" and "elevation") are possible, displayed in fig.31 and fig.32 as continuous and dashed lines, respectively.

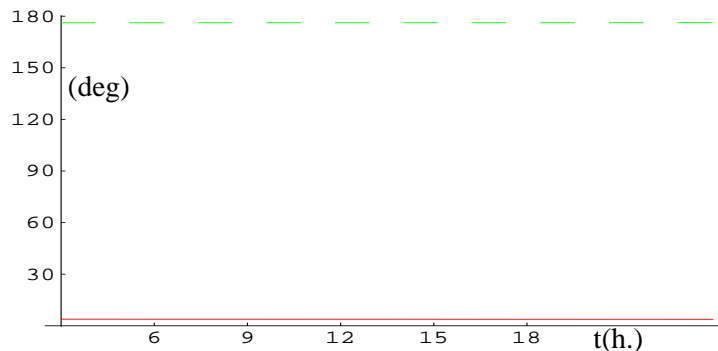


Fig. 31. HGA azimuth evolution

As observed qualitatively in projected geometry at Mars swing-by (fig. 25), Earth pointing is near to Mars pointing when approaching and opposite when receding. Consequently azimuth values (fig. 31) are near 0 deg for the first combination of pointing angles and near 180 deg for the second. Elevation values are firstly about -90 / -270 deg and later on +90 / -90 deg respectively for the two different combinations of pointing angles. Because of physical constraints on the rotation of the HGA's arm (see fig. 2) elevation is restricted to values between -210 deg and +60 deg, such that a rewinding of the HGA pointing would be required at closest approach if the ground link is to be maintained. Fortunately, this drawback does not take place during the interval of interest, that begins some hours after the closest approach time and one of the two pointing angle combinations can be used (see fig.31 and fig.32).

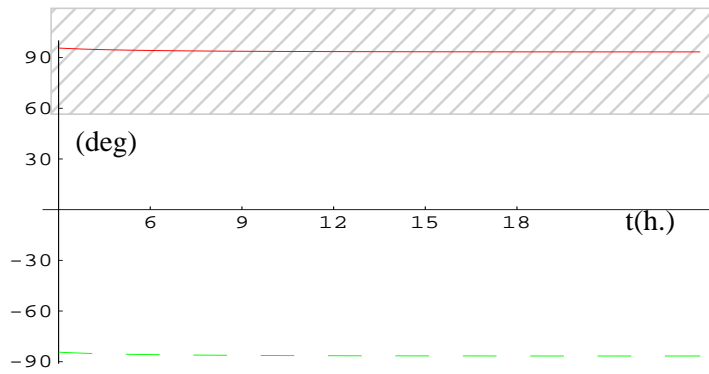


Fig. 32. HGA elevation evolution

5.2. Phobos tracking

Phobos is the inner moon of Mars and in the nominal case ROSETTA closest approach to Phobos (~9070 km) happens about fifteen minutes after closest approach to Mars. Phobos maximum axis (27 km) ensures an adequate apparent angular radius to detect (fig. 33). Estimates of the brightness may be found in (Ref. [4]).

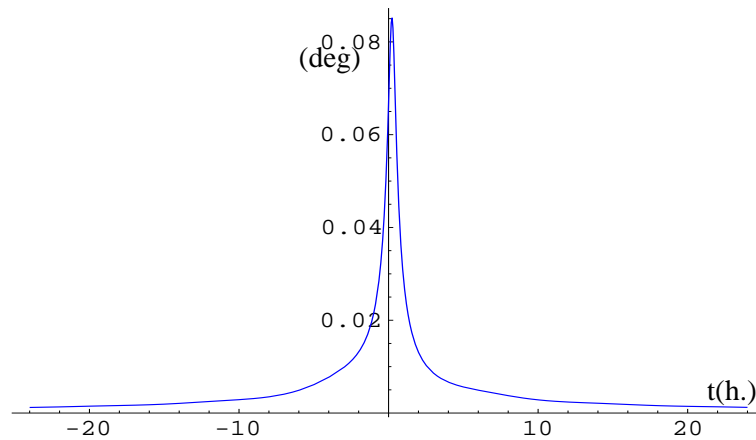


Fig. 33. Phobos apparent angular radius

Because of the Phobos orbital period of 7 h 39 min and its closeness to Mars only during two intervals of about 2.5 h Mars is out of fov of the NAVCAM (see fig. 34). During the first interval there is however sun incidence on the camera and on -X side and on +/- Y faces (fig. 35).

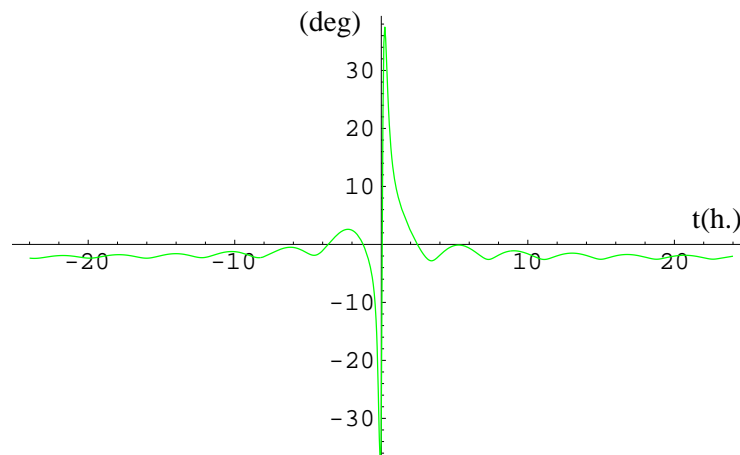


Fig. 34. Angular distance from Mars limb to Phobos tracking FOV

The second interval is also not usable since it contains a too high angular rate peak and the thermally critical - X side is again not protected from sunlight (see second peak on fig.35). Thus, Phobos tracking seems to be unfeasible for these conditions.

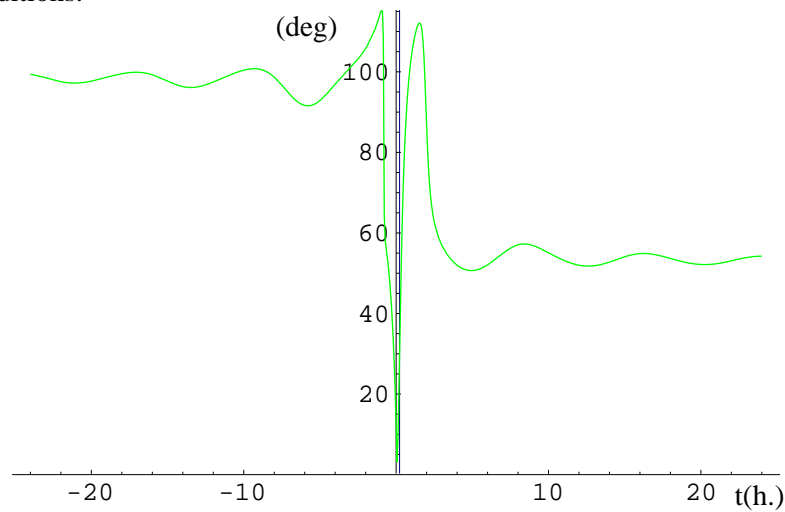


Fig. 35. Angle between sunwards direction and X-axis (Phobos nominal case)

Additionally, considering its short orbital period, Phobos could be anywhere in its orbit when ROSETTA passes through the closest approach for a generic case according to the mission uncertainties.

5.3. Deimos tracking sensitivity analysis

The orbital period of Deimos, the outer moon of Mars, is 30.3 hours. Taking into account the *a priori* timing uncertainty related to ROSETTA mission it is advisable to attempt a sensitivity analysis to determine whether there could be reasonable possibilities of tracking or not. For this purpose a series of eight graphs are drawn for each of the next figures, thicker and darker lines correspond to later dates of closest approach. The time interval between the graphs is one eighth of the Deimos orbital period (i.e. ~ 3.79 h.).

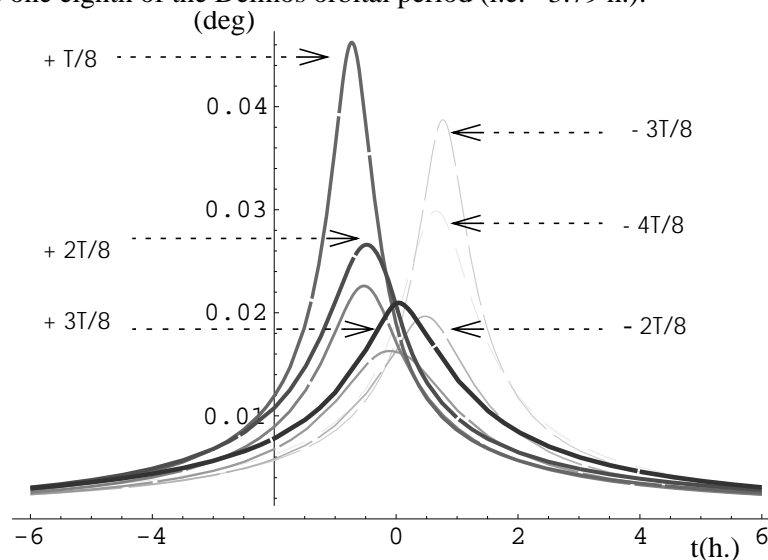


Fig. 36. Deimos apparent angular radii

Logically the angular radius varies similarly for all the subcases, achieving its top at the respective closest approach to Deimos, around Mars closest approach time. Recalling that the NAVCAM pixel resolution is 17.6 arcsec, Deimos longest axis is only projected on more than 1 pixel from about -6 h. to +6 h. w.r.t. the closest approach to Mars (fig. 36). For the brightness of Deimos see ref.4.

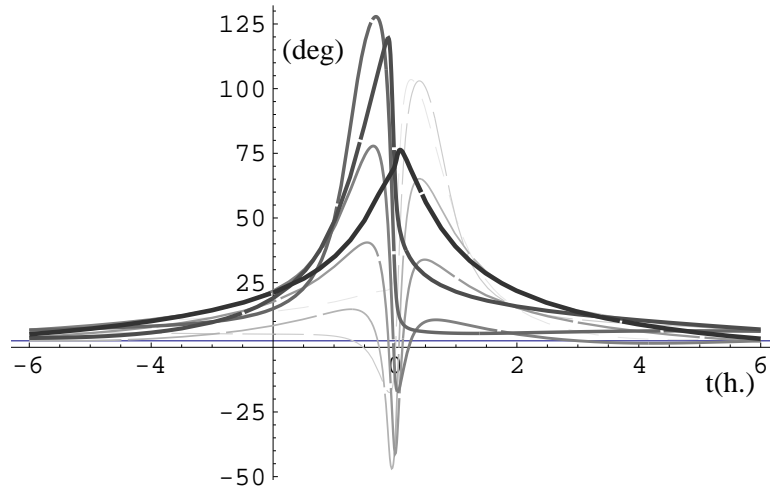


Fig. 37. Angular distance between Mars and Deimos limbs

As shown in figure 37., Mars and Deimos contours separation is under 15 deg up to $t=-4$ h and from $t=+4$ h onwards. For some subcases the separation is even under 2.5 deg and simultaneous appearance of Mars and Deimos on the fov of the NAVCAM occurs. For other subcases the low separation may be also undesirable because of straylight effects. Furthermore, excepting the three phases corresponding to the most advanced closest approach dates, Deimos becomes briefly occulted around the closest approach to Mars, as may also be observed from fig. 25.

The evolution of phase angle w.r.t. Deimos is shown in fig. 38. Because the sunwards direction is rather constant within the studied period (two days), results are evidently quite similar to the Mars tracking case since the pointing direction to either one or another target does not differ much except around the closest approach. Again, tracking after the closest approach to Mars is more favourable. Additionally, it could be shown that inadmissible angular acceleration peaks appear just before closest approach.

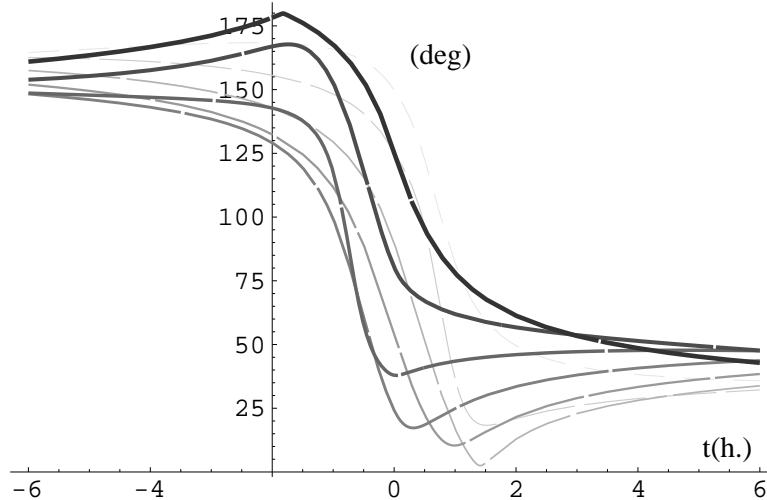


Fig. 38. Phase angle w.r.t. Deimos (sensitivity analysis)

When tracking after closest approach, sun incidence on - X side is not problematic for any subcase from $t = +1.5$ h onwards if the sign of the Y-axis (eq.3) is chosen conveniently, as shown in fig. 39.

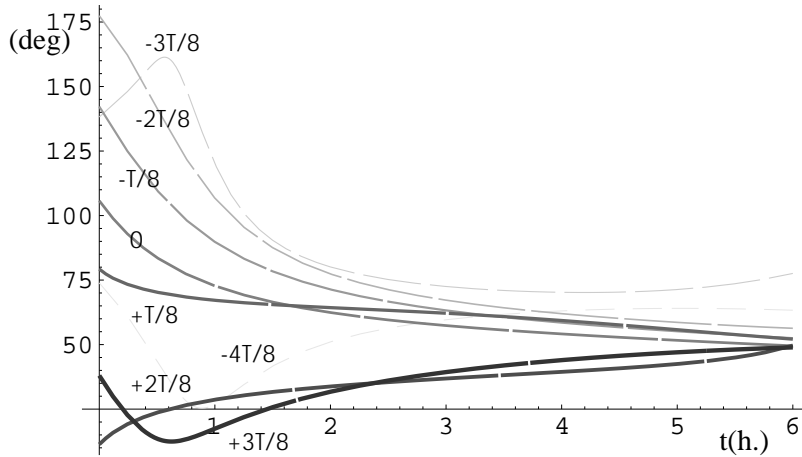


Fig. 39. Angle between sunwards direction and X axis (Deimos sensitivity analysis)

Solar incidence on +/- Y sides is quite variable between subcases (fig. 40). This is due to the definition of the Y-axis, perpendicular to the instantaneous relative position and to the commanded direction, (taking for instance as representative direction the relative velocity unit vector at +2 h after closest approach to Mars). The resulting Y-axis differs significantly from one Deimos phase to another. If the maximum allowable solar incidence on +/- Y faces were 30 deg. (TBC), most of the subcases would be within the ranges, as shown in fig.40. If limitations were though more restricting, some subcases should be discarded.

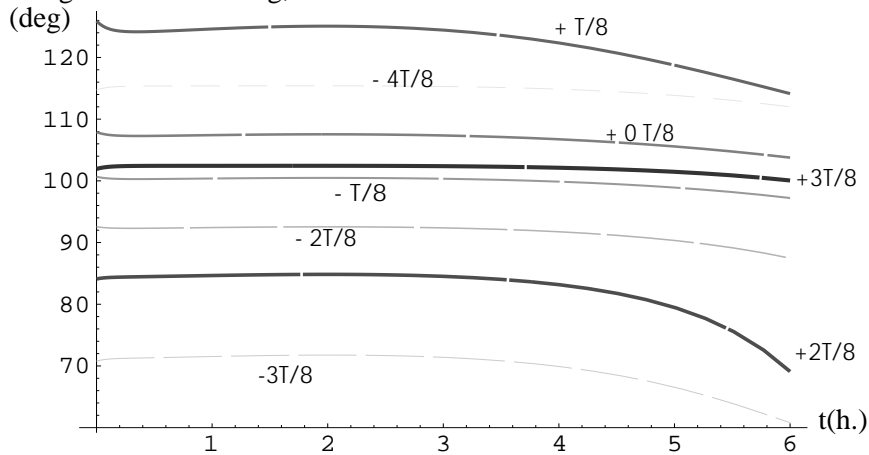


Fig. 40. Angle between sunwards direction and Y axis (Deimos sensitivity case)

Fig.41 and fig.42 show HGA pointing results, which are qualitatively similar to Mars case. Once again, one of the two possible pointing angle combinations could be used throughout the interval of interest.

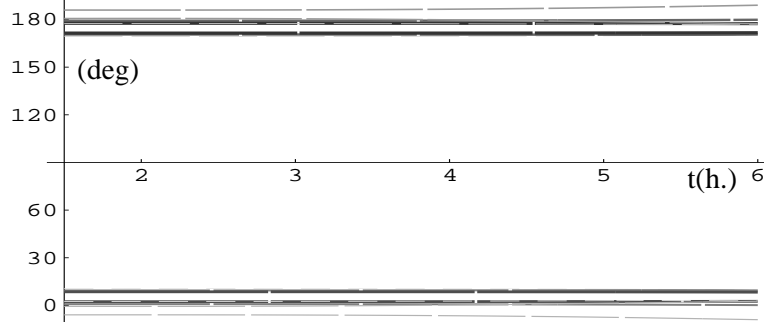


Fig. 41. HGA azimuth evolution

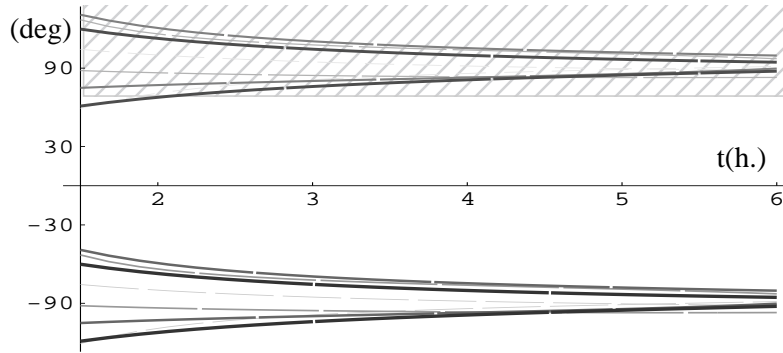


Fig. 42. HGA elevation evolution

As seen along this subsection, Deimos results are similar to Mars case but allowing tracking from $t = +1.5$ h. (Mars tracking period begins at $t = +3$ h because of excessive angular apparent radius).

6. CONSIDERATIONS ON APPLYING AFM FOR CASES OTHER THAN THE NOMINAL.

The design of the Asteroid Fly-by Mode assumes that ROSETTA trajectory w.r.t. the target is a straight line (refs. 2, 3).

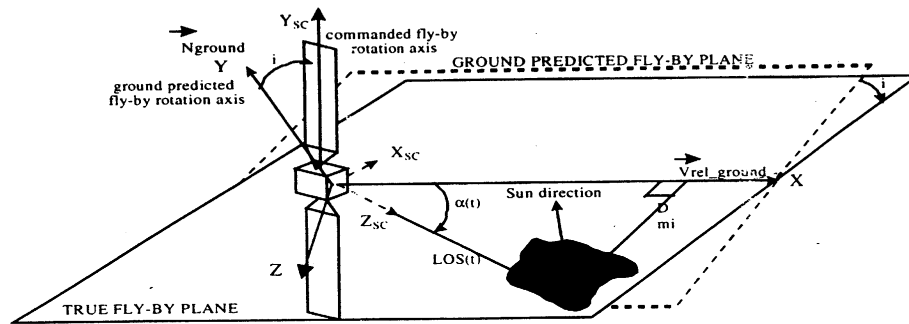


figure 6-2

Fig. 43. AFM design conditions

Ref.2 states: "the tracking motion is defined by the time evolution of the angle α between the relative velocity vector and the LOS vector to the asteroid". The Y-axis is the common perpendicular to the instantaneous relative position \vec{r} and to the ground estimate of the velocity unit vector commanded at the beginning of the autonomous fly-by phase $\hat{v}_{comm}/|\hat{v}_{comm}|$, which is representative of the relative velocity direction throughout the fly-by:

$$\hat{e}_y = \mp \frac{\vec{r} \times \hat{v}_{comm}}{|\vec{r} \times \hat{v}_{comm}|} \quad (15)$$

"The relative velocity direction is not updated by the guidance process, because it can be shown that its knowledge error is small enough" (Ref. [2]). This assertion, wholly demonstrated for the Asteroid Fly-by Mode (Ref. [3]), is no longer appropriate for curved trajectories, such as the swing-by trajectories around the closest approaches to the Earth and to Mars. For each one of these cases there is not a representative velocity direction for the complete manoeuvre to command in advance. For instance, if the relative velocity unit vector at closest approach is commanded, then some instantaneous relative positions appear very near to this direction of reference, as shown in fig. 44. This may influence negatively in the tracking process as defined above.

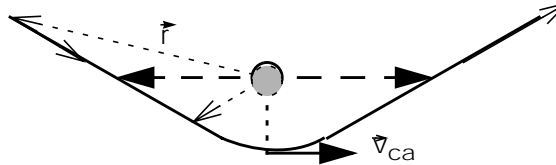


Fig. 44. Tracking motion for a general case.

When far enough from closest approach a representative velocity unit vector of the corresponding part of the trajectory may be used, e.g. the corresponding asymptotic velocity unit vector.

On the other hand, all the constraints could be more easily fulfilled at the same time if a convenient reference direction is commanded instead of a relative velocity unit vector at a given time. For instance, when commanding the sun direction, the angle between Y-axis and sunwards direction is 90 deg and +/- Y sides result always protected. However, the ability of the AFM to cope with this modification of the reference direction is to be confirmed.

For illustrative purposes, improvements on Moon tracking at first Earth swing-by are shown when commanding, for instance, sun direction as reference direction instead of the relative velocity unit vector at closest approach to Moon. Apart from protecting +/- Y sides, solar array rotation is also benefited. Fortunately - X face remains shaded as well, as shown in fig.45

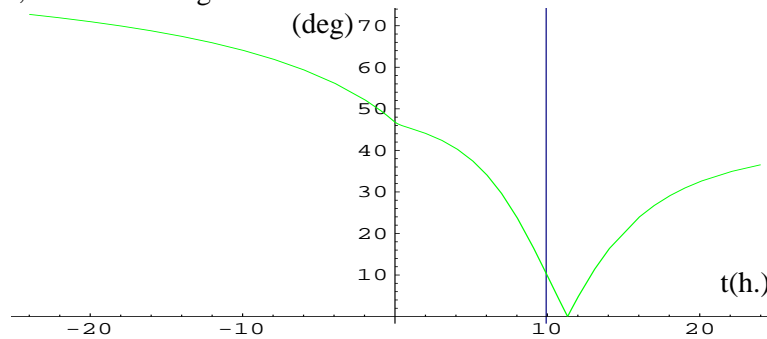


Fig. 45. Angle between sunwards direction and X-axis (->Moon I, modified)

The corresponding rates are significantly higher, especially on X -axis and Z-axis, but quite below the limits (fig. 46). Accelerations are also within the prescribed ranges. The results for the rest of constraints (NAVCAM fov and the phase angle) are not altered as independent of the Y-axis definition.

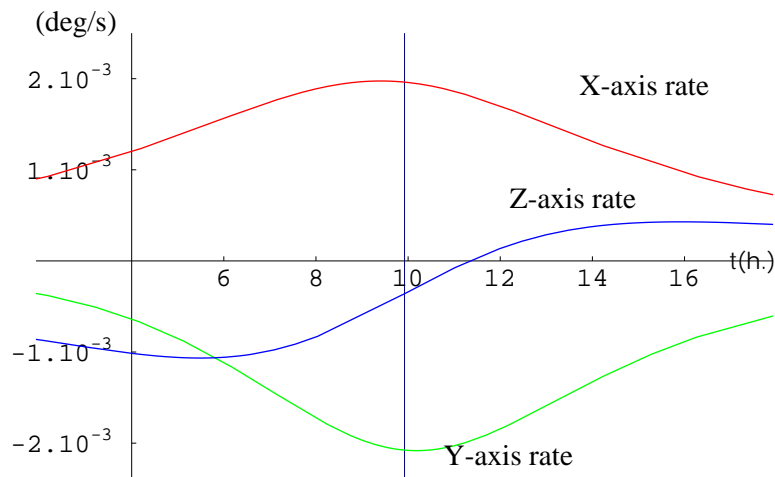


Fig. 46. Angular rates when pointing to Moon (I, modified)

7. CONCLUSIONS

Based on the known geometry of ROSETTA mission and according to the attitude prescriptions of the Asteroid Fly-by Mode (AFM), an analysis of opportunities to verify this mode in-flight has been presented.

In principle it seems certain that no clear opportunity is detected such that all the constraints become fulfilled simultaneously and such that the resulting situation is fully representative of an actual asteroid fly-by (Table 6). In general terms rotation requirements on the spacecraft and on solar arrays, (and on High Gain Antenna for the case of Mars too), are not as critical as the sun incidence requisites on the navigation camera, on -X side and, especially, on +/- Y faces.

The most promising case is the Moon tracking at first Earth swing-by during some hours before ROSETTA closest approach to the Moon. It additionally exhibits the advantage of an almost straight relative trajectory (fig. 4), more similar to the asteroid fly-by case. Unfortunately in these conditions there is a 45 deg sun incidence on the thermally sensitive - Y face of the spacecraft. Similar consequences are derived for the Moon tracking at second Earth swing-by during a more restricted interval. (In any case the second Earth swing-by occurs after Otawara fly-by and is thus of little interest for AFM check-out)

In table 6 a qualitative summary of the evolution of constraints fulfilment is displayed by six marks within every case (three before the closest approach to the target, three afterwards): where "+" stands for "fulfilled" and "X" for "not fulfilled"

Table 6. Synopsis of constraints fulfilment for Moon, Earth and Mars.

	Moon (I)	Earth(I)	Moon(II)	Earth(II)	Mars
	→	→	→	→	→
fov range	+++++	++XX++	+++++	++XX++	++XX++
Isolated target on fov	+++++	+++++	+X++++	++XX++	+++++
Angular rates	+++++	+++++	+++++	+++++	+++++
Angular accelerations	+++++	+++X++	+++++	+++X++	+++++
Phase angle	XX++++	XXX+++	+++++	XXX+++	XXX+++
Sun on -X face	XX++++	XXXX++	X+++XX	XXXX++	XXXX++
Sun on +/- Y Faces Incidence Angles (Allowed limit TBD)	15° - 45°	4°	20°	23°	11°

Earth pointing is more problematic at both swing-bys. The phase angle is not favourable before the closest approach. The field of view of the navigation camera is exceeded around the closest approach. Therefore, Earth imaging could be only started some hours after closest approach and it is very doubtful that tracking a receding target is appropriate to verify the Asteroid Fly-by Mode. Furthermore, for this part of the trajectory the pointing motion is little representative of the asteroid fly-by tracking. Likewise Mars presents the same disadvantages.

Phobos is not a suitable target since it appears too close to Mars and its short orbital period yields numerous occultations (subsection 5.2), apart from undesirable sun incidence.

Deimos configurations for different arrival dates have been discussed. Depending on the allowed solar incidence on +/- Y sides (TBC), more or less configurations could be propitious. Anyway, results are similar to Mars case and, once again, tracking would be only feasible when receding from the target, although now the relative motion of the target w.r.t. ROSETTA would be more significant.

Finally, commanding certain reference directions, different from a relative velocity unit vector at a given time, appears to be more promising. Following this strategy tracking of the Moon at first swing-by is possible. *Nevertheless, further implications of this approach on the complete tracking algorithm is not clear and its feasibility has to be confirmed.*

8. APPENDIX: ANGULAR RATES WHEN POINTING TO A TARGET

In a general case let \vec{u} be a unit vector attached to the spacecraft. Its derivative is given by eq.16: ‘

$$\dot{\vec{u}} = \vec{\omega} \times \vec{u} \quad (16)$$

where $\vec{\omega}$ is the S/C angular velocity.

In our case the Z-axis is already defined as the tracking direction:

$$\vec{e}_z = \frac{\vec{r}}{|\vec{r}|} \quad (17)$$

The derivative of the Z-axis results then in:

$$\dot{\vec{e}}_z = -\vec{v} \frac{1}{|\vec{r}|} - \vec{r} \frac{d\left(\frac{1}{|\vec{r}|}\right)}{dt} \quad (18)$$

On the other hand, as shown in expression 16:

$$\dot{\vec{e}}_z = \vec{\omega} \times \vec{e}_z \Rightarrow \vec{e}_z \times \dot{\vec{e}}_z = \vec{e}_z \times (\vec{\omega} \times \vec{e}_z) = \vec{\omega} - (\vec{\omega} \cdot \vec{e}_z) \vec{e}_z \quad (19)$$

the total angular velocity can be rewritten as:

$$\vec{\omega} = \vec{e}_z \times \dot{\vec{e}}_z + \omega_z \vec{e}_z \quad (20)$$

where the cross-product corresponds to:

$$\vec{e}_z \times \dot{\vec{e}}_z = \frac{\vec{r}}{|\vec{r}|} \times \left(\vec{v} \frac{1}{|\vec{r}|} + \vec{r} \frac{d\left(\frac{1}{|\vec{r}|}\right)}{dt} \right) = \frac{\vec{r} \times \vec{v}}{\vec{r} \cdot \vec{r}} \quad (21)$$

Inserting it in eq.21 yields:

$$\vec{\omega} = \frac{\vec{r} \times \vec{v}}{\vec{r} \cdot \vec{r}} + \omega_z \vec{e}_z \quad (22)$$

Equation 22 shows that the angular velocity can be separated in two terms. The first term is orthogonal to the orbital plane and corresponds to the minimum angular rotation necessary to point towards a target. It leads to the rates on X-axis and Y-axis. The second term represents an additional rotation around the direction to the target.

9. ACRONYMS AND ABBREVIATIONS

AFM	Asteroid Fly-by Mode
AOCMS	Attitude and Orbit Control and Measurement System
APM	Antenna Pointing Mechanism
AU	Astronomical Unit
c.a.	Closest approach
comm	commanded
CCD	Charge Couple Device
fov	field of view
HGA	High Gain Antenna
LOS	Line of Sight
min.	minimum
NAVCAM	Navigation Camera
SA	Solar Array
S/C	Spacecraft
TBC	To be confirmed
w.r.t.	with respect to

10. ACKNOWLEDGEMENTS

The work described in this paper was supported by GMV S.A., under a contract with ESOC. Special thanks to Mr. Companys, Mr. Morley and Mr. Fertig for the supervision from ESOC/Flight Dynamics-Interplanetary Missions. The idea to consider reference directions other than the nominal comes from Mr. Companys. Figures 3, 4 and 25 come from Mr. Morley.

11. REFERENCES

- [1] Pellón Bailón, J.L., Rodríguez Canabal, J., Yáñez Otero, A.: "ROSETTA -Consolidated Report on Mission Analysis " , RO-ESC-RP5500 ESA/ESOC ,(February 1999).
- [2] Lacuisse,C.: "Asteroid Fly-by Mode: Definition and Justification", RO-MMT-TN-2040, Issue 1, MMS (April 1999)
- [3] Lacuisse,C.: "Asteroid Fly-by Mode Analysis", RO-MMT-TN-2017, Issue 1, MMS, (September 1998)
- [4] Morley, T.: "Mars Swing-by Geometry and Conditions for Optical Navigation", RO-ESC-TN-5507, Issue 1, ESA/ESOC, (January 1999)
- [5] Morley, T.: "On the Asteroid Fly-bys and Optical Navigation", RO-ESC-TN-5502, Issue 1, ESA/ESOC, (June 1998)
- [6] Juillet, J.: "ROSETTA Design Report", RO-DSS-RP-1004, Issue 2 , DSS, (September 1998)
- [7] Fertig, J.: "ROSETTA Navigation Camera: Operational Considerations", 980402 (June,1999)
- [8] Fertig, J.: "ROSETTA Navigation Camera: Exposure Time as Function of Geometry", 980402 (June,1999)

- [9] Müller, M., Grün,E.: "ROSETTA - An Engineering Model of the Dust and Gas Environment of the Inner Coma of Comet P/Wirtanen", RO-ESC-TA-5501, Draft 0, ESA/ESOC (1997)
- [10] Allen, C.: 1973, "Astrophysical Quantities ", 3rd. Edition, The Athlone Press.
- [11] Seidelmann, P. "Explanatory Supplement to the Astronomical Almanac", University Science Books. (1992)
- [12] Elices, T.: "Introducción a la Dinámica Espacial", Instituto Nacional de Técnica Aeroespacial (1991).